Loss mechanisms in femtosecond laser written optical waveguides

Paulo V. S. Marques*[a,b], Vitor A. Amorim[a,b], João M. Maia[a,b], Duarte Viveiros[a,b]
[a] Department of Physics and Astronomy, Faculty of Sciences, University of Porto, Porto 4169-007, Portugal;
[b]CAP - Centre for Applied Photonics, INESC TEC, Porto 4150-179, Portugal

ABSTRACT

Low loss optical waveguides are the key component for the fabrication of more complex integrated optics devices. In most works related to femtosecond laser written waveguides, the values presented give results at a single wavelength or in a narrow wavelength band; but some applications in optical sensing, for example, would benefit from waveguides having good propagation properties in a larger wavelength range. This paper presents results that allow one to gain insight into the major loss mechanisms present in laser written waveguides in two different types of glasses (fused silica and Eagle 2000 glass) and the dependence of those on the fabrication parameters. Finally, an example of application of broadband operating waveguides is given.

Keywords: Fentosecond laser direct writing, integrated optics, optical waveguides, propagation loss, Mie scattering, Raleigh scattering

1. INTRODUCTION

Optical waveguides in the context of integrated optics have been traditionally fabricated by photolithographic techniques due to its technological maturity. The possibility to directly inscribe optical waveguides in glasses using a femtosecond laser was first demonstrated by Davis et al. [1]. While photolithographic techniques offer significant advantages in scalability, cost, and circuit footprint, femtosecond laser direct writing can offer prototyping flexibility without the need for masks or multiple fabrication steps, and three-dimensional geometries that are not possible in traditional fabrication methods. The latter has been used in several materials such as glasses, crystals, and polymers, and already enabled the fabrication of many integrated optical devices, including buried waveguides [2], Bragg grating waveguides [3], directional couplers [4], Y-junctions [5], integrated lasers [6], add-drop multiplexers [7], arrayed waveguide gratings [8], among others. Femtosecond laser direct writing can also benefit the ongoing exponential growth trend in data communications. The implementation of multicore fibers to scale the information transmitted by the number of cores, requires devices matching the out-of-plane characteristics of those fibers. It has been reported that this inherently 3D technique has already been implemented in the fabrication of three-dimensional fan-out devices for multicore fiber coupling applications [9]. On very specific materials such as fused silica, this technique also enables the monolithic integration of optical waveguides together with microfluidic channels in a 3D fashion for on-chip optical sensing [10, 11]. Although infrared wavelengths are the most relevant for optical communications, shorter wavelengths are indeed important for applications like optical sensing relying on plasmonics or absorption measurements [12, 13]. Since shorter wavelengths are more affected by defects present in the waveguides [14, 15], understanding its loss mechanisms and their dependence with fabrication parameters is key to improve their quality as well as to maximize the performance of said devices.

In this paper we report a systematic study concerning the origin of the losses for femtosecond laser writing of optical waveguides in fused silica [16] and alkaline earth boro-aluminosilicate glass substrates (Eagle2000) [17] in a wavelength band ranging from the visible to the infrared just above the third telecommunication window. In this study, several waveguides were fabricated while varying fabrication parameters such as pulse energy and scanning velocity. The coupling and propagation losses (Rayleigh and Mie scattering parameters) were determined for both type of waveguides; this characterization improved our understanding on the dynamics of the scattering processes inherent to the waveguide fabrication, allowing to determine the optimal processing window for the fabrication of low loss broadband waveguides.

*psmarque@fc.up.pt; phone (+351) 22 0402301; www.inesctec.pt

2. EXPERIMENTAL PROCEDURES

A fiber amplified femtosecond laser (Amplitude Systèmes Satsuma HP), with a second harmonic beam at 515 nm and a pulse duration of approximately 250 fs at 500 kHz, was used to induce the refractive index modification in glass substrates. Laser modification tracks were formed by transverse scanning the substrate on Aerotech air-bearing linear stages (ABL10100-LN), with the linearly polarized beam focused at a depth of 100 µm via a 0.55 numerical aperture aspherical lens (New Focus 5722-A-H) mounted in a vertical piezo stage (PI P-725.4CD PIFOC). Laser beam polarization was set parallel to the writing direction, and all waveguides were written on the same scanning direction to avoid the Quill effect [18].

The side facets of all substrates were polished after writing in order to eliminate laser damage induced in the substrates' input and output facets, and to remove the waveguide tapered region created by the influence of the substrates' edge on the beam focus.

To determine the spectral characteristics of the fabricated devices, the broad spectrum of a halogen lamp was coupled into a single-mode fiber (SMF-28) and butt-coupled to the entrance facet of the modification tracks. The substrate was mounted on an Elliot Martock MDE881 stage with piezo controls (Dali E-2100) and special holders for precise alignment of the input/output optical fibers. The light collected by a second butt-coupled optical fiber at the exit facet was inspected in an optical spectrum analyzer (ANDO AQ-6315B) from 500 nm to 1700 nm with a 10 nm resolution. All transmission spectra were normalized to the source spectrum to obtain the insertion loss. Index matching (Cargille series: AA $n_D^{25ºC} = 1.458 \pm 0.0002$) was used to minimize Fresnel reflections at both input/output fibers/facets.

Sample annealing, when employed, was made during 2 hours at the target annealing temperature, using a 15ºC/min heating ramp, on a Carbolite RHF 1500 furnace.

3. RESULTS AND DISCUSSION

The work presented here was focused on the losses of two different types of glasses; on one hand a fused silica substrate and on the other hand a softer alkaline earth boro-aluminosilicate glass substrate (Eagle2000).

3.1 Waveguides on fused silica substrates

The waveguides on a fused silica substrate were fabricated with energies ranging from 40nJ to 400nJ and velocities ranging from 100 µm/s to 6400µm/s. A second group of similar waveguides was subjected to a thermal treatment at 800, 900, 1000, and 1200ºC. Fig. 1 displays the cross-section and top views of waveguides fabricated with different exposure energy levels and two different velocities, namely 100 µm/s and 3200 µm/s (waveguides fabricated with a scan velocity of 6400 µm/s as well as waveguides annealed at 1200ºC were not considered due to the very weak light guidance). The elongated modification induced by the focused femtosecond beam is typical, with the modified volume dimensions increasing significantly with pulse energy and diminishing slightly at higher scan velocities. The spectral transmission characteristics also depend on pulse energy and scan velocity, as can be seen in Fig. 2(a) and (b) respectively. In the first case, the insertion losses at longer wavelengths become smaller as pulse energy increases, but shows no clear dependence with pulse energy at shorter wavelengths. The losses also increase when the velocity increases for the entire range of velocities tested. Insertion loss decreases with increasing annealing temperature for shorter wavelengths, Fig. 2(c), but unfortunately increases for longer wavelengths. The same behavior was observed by Bhardwaj et al. at 633 nm [19].

To better understand the processes underlying the spectral behavior, the cut-back technique was used, and the total insertion loss (IL) was measured for the three different lengths available (1.3, 2.2, and 3.3 ± 0.1 cm). From the plot of the insertion loss of each waveguide as a function of sample length for each wavelength we were able to retrieve both propagation (slope) and coupling loss (y-axis interception) by using the following equation:

$$IL(\lambda) = PL(\lambda) + 2CL(\lambda) \tag{1}$$

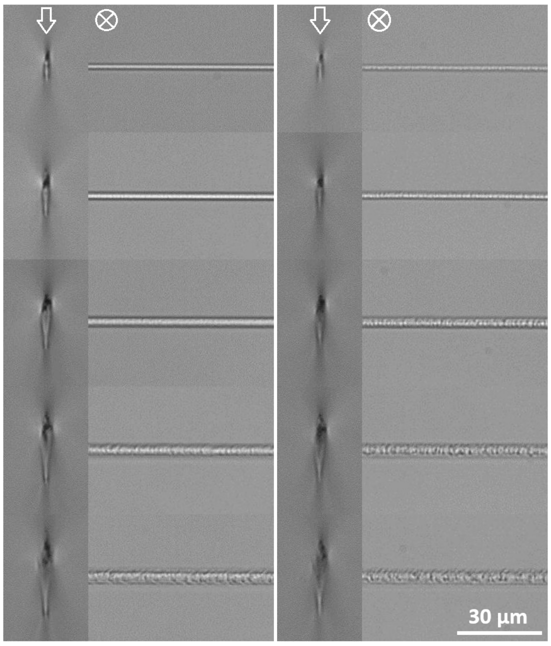

Fig. 1. Transmission mode optical microscope images of the cross-section and top views of waveguides written in fused silica with pulse energies of 50, 100, 200, 300, and 400 nJ (top to bottom, respectively), for a scan velocity of 100 µm/s (left) and 3200 µm/s (right). Arrows indicate the laser beam propagation direction.

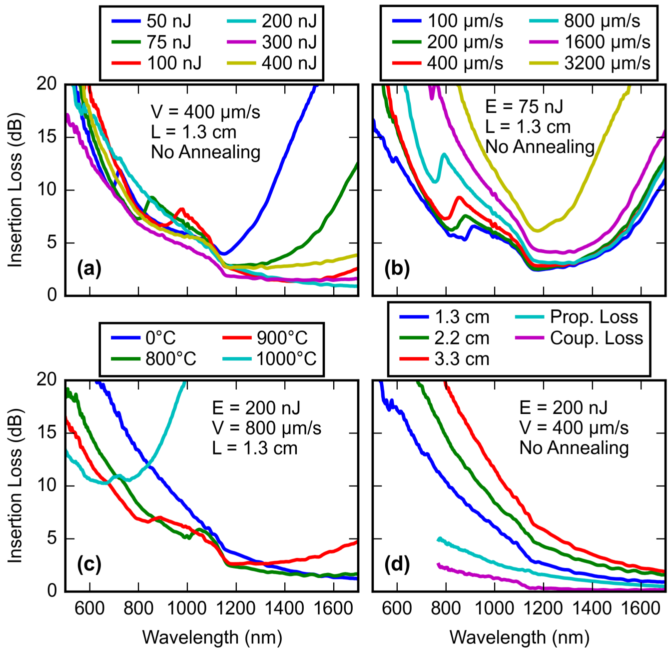

Fig. 2. Insertion loss of the fabricated waveguides as a function of wavelength for varying pulse energy (a), scan velocity (b), and annealing temperature (c). (d) Insertion loss of a waveguide for different lengths, together with propagation and coupling loss plotted in dB/cm and dB/facet, respectively.

Fig. 3 displays the obtained coupling and propagation losses. From Fig. 3(a-c), it is possible to see that there are three main occurrences of interest. The first is the immediate increase in coupling losses at approximately 1150 nm; at this wavelength the butt-coupling fibers become multimode, increasing the mode mismatch and, therefore, the coupling losses due to mode mismatch. The second is the monotonic growth in coupling losses, at longer wavelengths, as wavelength increases; here, the expansion of the guided mode translates into additional mode mismatch. The third occurrence of interest is the variation in coupling losses, at longer wavelengths, with the tested parameters. We conclude that, at longer wavelengths, coupling losses increase whenever the pulse energy is decreased, the scan velocity increased, or when the annealing temperature at which the waveguides were submitted is higher.

Previous studies evidenced the creation of nonbridging oxygen hole centers and self-trapped exciton (E_g') defects along with increased 3- and 4-membered rings in the silica network of femtosecond laser written waveguides. The increased 3- and 4-membered rings' concentration in the silica network are associated with material densification and are responsible for the higher refractive index, which increases with pulse energy [19-23]. While defects anneal out at a temperature as low as 150ºC, the increase in 3- and 4-membered rings' concentration is significantly more resistant to thermal treatment, only annealing out after heat treatment at 800-900ºC for long periods of time [24, 25]. These results match our observations, since a lower refractive index contrast together with lower physical waveguide dimensions, deriving from a smaller net writing fluence and/or higher annealing temperature, reduces the V-number, thereby increasing mode field diameter and, subsequently, mode mismatch, as it has already been observed by Shah et al. at 1550 nm [26]. This demonstrates the importance of the fabrication and heat treatment parameters in the guidance characteristics at long wavelengths, since low pulse energy, high scan velocity, and/or high annealing temperatures will lead to low quality waveguides in this region.

In Fig. 3(d-f) the monotonic increase in propagation loss, as wavelength decreases, is visible for all fabrication parameters tested. This behavior was already observed by Thomson et al., and was attributed to the possibility of loss being dominated by Rayleigh scattering [14]. Tong et al also showed that scattering plays a major role on femtosecond laser written waveguides, accounting for more than 90% of the propagation loss at 633 nm [15]. The C/λ^4 trend observed in Fig. 3(d-f) suggests a strong Rayleigh scattering influence in propagation loss. The losses do not depend strongly on the pulse energy, but when the scanning velocity increases the propagation loss follows, meaning that the Rayleigh scattering coefficient rises. The scattering losses are possibly due to sub-wavelength inhomogeneities which seem to smooth out with thermal treatment, Fig. 3(f). Despite Rayleigh scattering being the major contributor to propagation loss, an almost wavelength independent baseline loss also exists, which was attributed to Mie scattering.

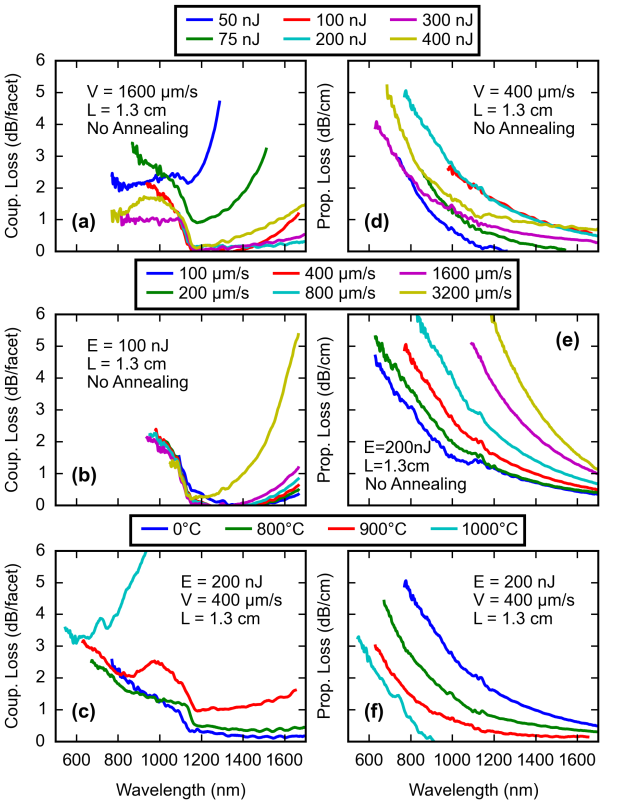

Fig. 3. Coupling and propagation loss of the fabricated waveguides as a function of wavelength for varying pulse energy (a, d), scan velocity (b, e), and annealing temperature (c, f).

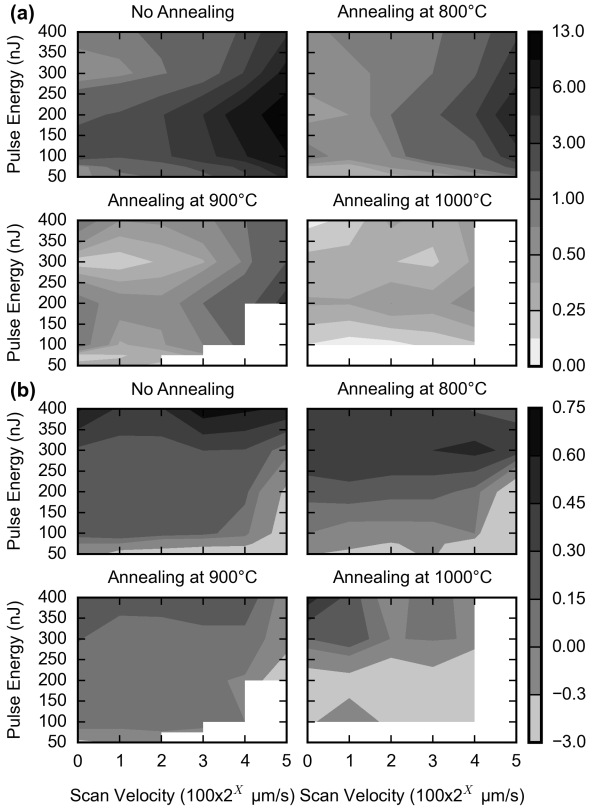

Fig. 4. Rayleigh (a) and Mie (b) scattering coefficients, in dB·cm^{-1}·µm^4 and dB/cm respectively, as a function of pulse energy and scan velocity for the different annealing temperatures.

The propagation loss data was modelled using equation (2) together with a python program employing the Levenberg-Marquardt algorithm to fit the Rayleigh and Mie scattering coefficients (C_{RS} and C_{MS}, respectively).

$$PL = \frac{C_{RS}}{\lambda^4} + C_{MS} \tag{2}$$

The Rayleigh scattering is seen to increase with scan velocity for all pulse energies tested, from a minimum of ≈ 0.5 to a maximum of 12.4 dBcm^{-1}µm^4. This tendency is successfully attenuated by applying thermal treatments at increasingly higher temperatures, with improvements being found even at low scan velocities. A minimum Rayleigh scattering coefficient of approximately 0.08 dBcm^{-1}µm^4 was found after a thermal treatment at 1000ºC. Pulse energy dependent behavior is also present, with higher Rayleigh scattering coefficients being found in waveguides fabricated at 200 nJ independently of the annealing temperature. The absence of data at high annealing temperatures, lower pulse energies, and high scan velocities, is due to the poor light guidance.

The extracted Mie scattering coefficients are plotted in Fig. 4(b). An increase in the Mie scattering coefficient of ≈ 0.2 to 0.65 dB/cm is seen as pulse energy increases while being relatively independent of scan velocity, suggesting that the Mie scattering most likely arises from an energy dependent process. However, as seen in Fig. 1, micron scale inhomogeneities created within the waveguide become more apparent either at higher pulse energy or higher scan velocity. This contradiction in scan velocity dependence most likely arises from the absence of a slowly varying spectral content at longer wavelengths. Also, a negative region is present whenever the scan velocity is high and pulse energy low, growing for higher annealing temperatures; this is clearly unrealistic and arises from the lack of a nearly constant spectral component at longer wavelengths, since, in these cases, the fitting is made with rapidly varying propagation loss data. An improvement of the Mie scattering coefficients can be achieved, to some extent, through thermal processing.

3.2 Waveguides on Eagle 2000 substrates

Similar to the study done for waveguides in fused silica, several optical waveguides were fabricated in a 75 mm long Eagle2000 substrate with pulse energy ranging from 50 nJ to 250 nJ and scan velocity between 1 cm/s to 8 cm/s. Fig. 5 displays the cross-section and top view of waveguides fabricated with different pulse energies for a scan velocity of 1 cm/s and 8 cm/s. As can be seen, these structures are composed by a central core delimited by a dark region and surrounded by an external cladding-like structure, which is typical for waveguides fabricated in the heat accumulation regime [27, 28]. The dimensions of the modified volume are seen to increase significantly with pulse energy, diminishing for higher scan velocities, indicating a significant dependence on laser net fluence.

The spectral characteristics of the optical waveguides also depend on pulse energy and scan velocity, as can be seen in Fig. 6. At low pulse energies, insertion losses are higher at shorter and longer wavelengths. For pulse energies up to 150 nJ, insertion loss at longer wavelengths is seen to decrease monotonically with increasing pulse energy and decreasing scan velocity; for this energy level, better results are achieved at higher scan velocities. The loss at shorter wavelengths is, on the other hand, maximized for intermediate pulse energies and smaller scan velocities, decreasing greatly for higher scan velocities independently of pulse energy. Furthermore, the spectrum of waveguides fabricated at high pulse energy (above 200 nJ) and low scan velocity (below 2.5 cm/s) is not easy to understand; the existence of peaks in the spectrum can be explained by the presence of multiple waveguiding regions to which the light couples as it propagates.

Again, to decompose the origin of the losses, the cut-back technique was used and the substrates diced into three different lengths (1.3, 2.3, and 3.2 ± 0.1 cm), with both propagation and coupling loss being retrieved from insertion loss fittings. Waveguides fabricated at high pulse energy and low scan velocity were discarded from this analysis, as their complex behavior yielded results with considerable error.

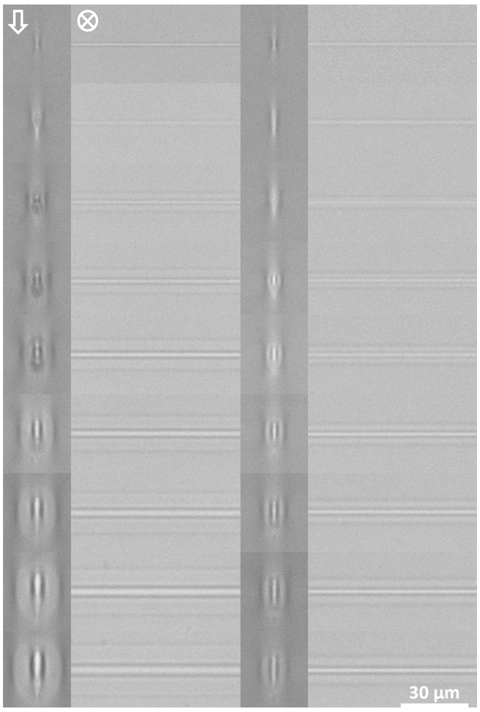

Fig. 5. Transmission mode optical microscope images of the cross-section and top views of waveguides written in fused silica with pulse energies of 50, 75, 100, 125, 150, 175, 200, 225, and 250 nJ (top to bottom, respectively), for a scan velocity of 1 cm/s (left) and 8 cm/s (right). Arrows indicate the laser beam propagation direction.

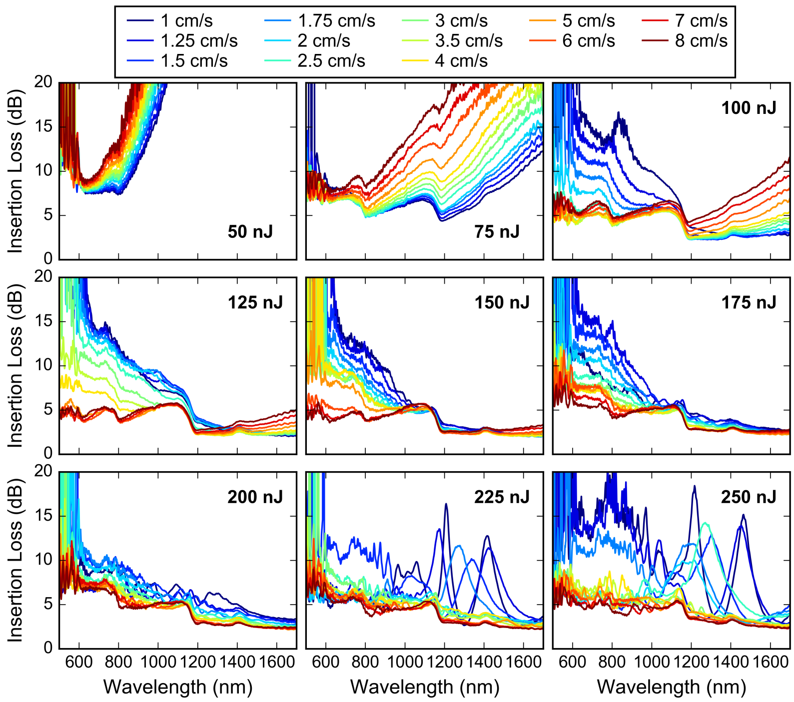

Fig. 6. Insertion loss of 2.3 cm long optical waveguides as a function of wavelength for varying pulse energy and scan velocity.

From the coupling and propagation losses for specific cases shown in Fig.7, it is possible to identify from Fig. 7(a, b) several regions of interest. The first is the monotonic growth in coupling losses for longer wavelengths due to guiding conditions closer to the cut-off condition and, therefore, increasing the mode field diameter, which translates into additional mode mismatch between the fiber and waveguide mode. These results match the results obtained for fused silica in fused silica, and can be explained by the dependence of the refractive index modification as well as the dimensions of the guiding region in pulse energy and scan velocity. The second is the existence of dips in the coupling loss spectra, as can be seen in Fig. 7(b) just before 800 nm and 1200 nm. These are related to the modal structure of the butt-coupling optical fibers, where each discontinuity corresponds to additional modes being supported at lower wavelengths. A more complex coupling behavior is also to be expected between optical waveguides fabricated with higher pulse energies and lower scan velocities, as these may support multiple modes at a given wavelength. Therefore, the coupling behavior will depend on the characteristics of the coupling optical fiber.

In Fig. 7(c), the monotonic increase in propagation loss as wavelength decreases is visible for all pulse energies tested. The variability observed across this wavelength range is caused by a dependency on the energy (as was observed for fused silica) which can be attributed to propagation loss being dominated by Rayleigh scattering. The propagation loss of such waveguides also depends on scan velocity, as can be seen in Fig. 7(d), with a significant decrease in loss at shorter wavelengths being observed for higher scan velocities. Furthermore, small variations in the propagation loss spectra are seen to blue shift as scan velocity increases (Fig. 7(d)). These variations represent the appearance of additional propagation modes as wavelength decreases, which causes the scattering to affect the modes in slightly different amounts. The blue shift of these transitions occurs due to a decrease in V-number from the decrease in refractive index contrast and waveguide dimensions. The same behavior occurs for decreasing pulse energy. Despite Rayleigh scattering being the major contributor to propagation loss, additional loss is also apparent from the C/λ^4 trend deviation, clearly seen in Fig. 7(d). This additional loss originates from the glass's bulk absorption [29], being created by the vibrational overtone of the hydroxyl group OH^- [30], with an absorption peak centered at 1385 nm, and by the ferrous ion Fe^{2+} [31], with a broad absorption peak at 1075 nm. An almost wavelength independent baseline loss also exists, which was attributed to Mie scattering.

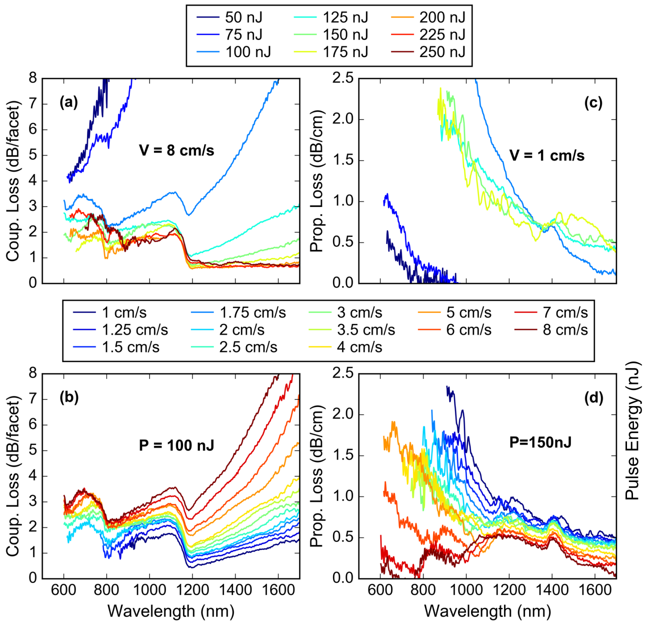

Fig. 7. Coupling and propagation loss as a function of wavelength for varying pulse energy (a, c) and scan velocity (b, d).

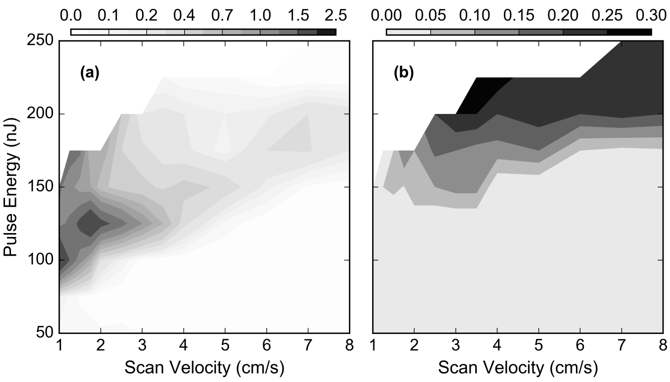

Fig. 8. Rayleigh (a) and Mie (b) scattering coefficients, in $dB{\cdot}cm^{-1}{\cdot}\mu m^4$ and dB/cm respectively, as a function of pulse energy and scan velocity.

Propagation loss at longer wavelengths is dominated by the bulk absorption of Eagle2000 ($BA_{Eagle2000}$) [5]. As such, in order to properly retrieve the Rayleigh and Mie scattering coefficients (C_{RS} and C_{MS}, respectively), the propagation loss data was modelled using equation (3), which takes the bulk absorption into account.

$$PL(\lambda) = \frac{C_{RS}}{\lambda^4} + C_{MS} + BA_{Eagle2000}(\lambda) \tag{3}$$

The Rayleigh and Mie scattering coefficients are plotted in Fig. 8. It should be noted that the coefficients extracted from waveguides fabricated at low pulse energies and high scan velocities are estimated, as the large coupling loss variations at longer wavelengths give rise to higher propagation loss uncertainty. Rayleigh scattering, Fig. 8(a), is seen to decrease with scan velocity for all pulse energies tested, from a maximum of approximately 2 $dBcm^{-1}\mu m^4$ to a negligible value (<0.05 $dBcm^{-1}\mu m^4$). Pulse energy dependent behavior is also present, with higher Rayleigh scattering coefficients being found for waveguides fabricated at around 125 nJ and low scan velocity. This behavior is also perceptible from the transmission mode optical microscopy images present in Fig. 5, where less light is seen to reach the end facet of waveguides fabricated with these parameters, improving for high scan velocities. The extracted Mie scattering coefficients are plotted in Fig. 4(b). From the data, an increase in the Mie scattering coefficient from ≈ 0 to 0.3 dB/cm is seen as pulse energy increases, being relatively independent of scan velocity. This behavior suggests that Mie scattering most likely arises from an energy dependent process. Curiously, there are no micrometer scale inhomogeneities visible within the waveguides, as seen in Fig. 5, that can explain these results.

The results obtained in this work are comparable to those achieved by Eaton et al. [32] in the telecommunications band and in the same material: Rayleigh scattering coefficients ranging between 0.8 and 1.7 $dBcm^{-1}\mu m^4$ and a Mie scattering coefficient of ≈0.16 dB/cm were found for a scan velocity between 0.8 and 2 cm/s and a pulse energy of 133 nJ at 1.5 MHz. As in this work, the authors found that the Mie scattering was independent of scan velocity and that the Rayleigh scattering decreases for higher scan velocity. Also, by using a higher scan velocity we were able to reduce the Rayleigh scattering by an order of magnitude in relation to the results above. These results are also an improvement in relation to the ones obtained in fused silica, as decreasing the Rayleigh scattering through thermal treatment increases the coupling losses at longer wavelengths dramatically. Mie scattering is also lower in the case of Eagle2000, with a two to three order of magnitude higher scan velocity being possible.

4. APPLICATION EXAMPLE

Several sensing applications of integrated optics rely on evanescent interaction of guided light with the external medium, therefore changing the light phase. This phase change could be then transformed into intensity modulation by means of an interferometer, for example; additionally, a resonant structure could be incorporated within the interaction zone and changes on refractive index are translated into a wavelength change. In some of those situations the wavelength region of interest is on the visible spectrum and therefore having broadband operating waveguides is of paramount importance. The device described in this section relies on the evanescent excitation of plasmons on a metallic film deposited on the surface of an integrated optic chip; the excitation is achieved by a near surface waveguide, fabricated by femtosecond laser writing, Fig. 9 (right).

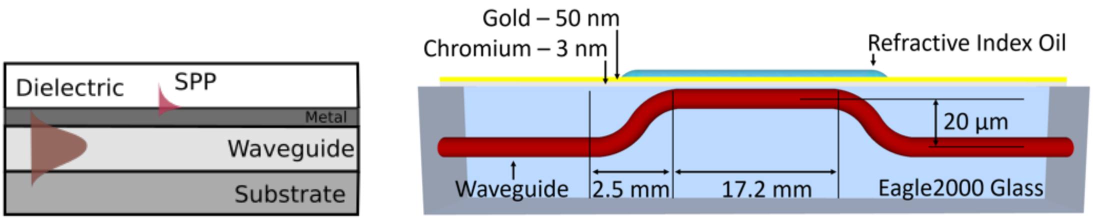

Fig. 9 – (Left) Schematic demonstrating the excitation of a surface plasmon using the evanescent field of a guided mode. (Right) Schematic of the SPR devices fabricated and studied in this work.

The main difficulty on achieving waveguides close to the surface is that the process is prone to surface ablation. Therefore, the solution is to write deep into the substrate and then etch back with a hydrofluoric acid (HF) solution to such an extent that the effective refractive index of the mode guided in the waveguide is modified by the refractive index of an external medium. In this study, a set of parallel waveguides were written below the surface at successive different depths (the depth difference between adjacent waveguides was 500 nm). This approach allows the fabrication of a set of waveguides at different depths and therefore with different coupling coefficients, enabling a complete study over this parameter.

The first etching tests were run on waveguides written in fused silica substrates, and the results are demonstrated on Fig. 10(a). The problem is that when the etching approaches the volumes of modified refractive index the etching progresses quickly without much control into the laser affected volume. It was registered that the waveguides are either destroyed by the etching or that the guided light on the remaining waveguides does not couple outside of the chip. Since the etching selectivity difference between pristine glass and femtosecond exposed glass is much higher for pure fused silica than other multicomponent glass, the same experiment was repeated for Eagle2000 substrates and the result is shown in Fig. 10(b). It should be pointed out that the etching chemistry for Eagle2000 glass is not exactly the same as the one used for fused silica. While fused silica uses a HF solution with different dilution levels, the same approach in Eagle2000 glass resulted in a poor surface quality arising from the multicomponent structure of the glass. Therefore, the etching recipe was adjusted by adding hydrochloric acid (HCl); it was determined that a 10:2 volume ratio of HF(1%):HCl(37%) was able to achieve an etched surface roughness of around five nanometers after a 80 minutes long etching process at 40ºC (etch rate ≅0.45μm/min).

(a) 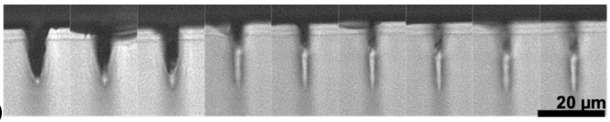

(b) 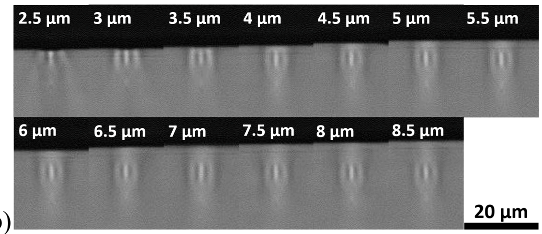

Fig. 10 – Transmission mode optical microscope images of the cross-section of optical waveguides translated to the surface of Suprasil 1 (a) and Eagle2000 (b) by wet etching. In (b), the surface to core center distance is depicted for each of the cross-sections.

Following the results of Fig. 10, a metallic film was deposited on the sample surface (3 nm of Cr followed by 50 nm of Au, like seen on Fig. 9 right). Fig. 11 depicts the spectra measured for the waveguides at different depths for an external medium with a refractive index of $n_D^{25ºC}$ =1.4580 ± 0.0002. The advantage of this scheme is that it is possible to measure different waveguides, each one of them with a different plasmonic coupling strength. As the light source used to obtain these spectra is not polarized, the maximum loss peak achievable is limited to 3 dB. In normal circumstances this would not be a problem; however, SPR peaks are broad and the insertion loss spectra of these devices quite complex, making it difficult to accurately detect the useful data. Therefore, a data treatment was required to extract the loss peak—induced by the excitation of the surface plasmon—from the remaining characteristics of the spectrum.

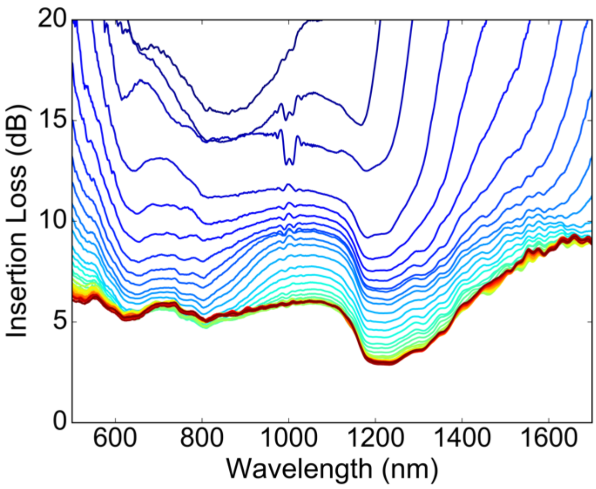

Fig. 11 - Insertion loss spectra of the devices when exposed to Cargille series: AA $n_D^{25ºC}$ =1.4580 ± 0.0002. The evolution from blue to red represents the transition from the shallowest optical waveguide to the deepest in steps of 0.5 μm.

One solution to this issue relies on the measurement of the insertion loss spectra of the devices in air, and then use these spectra as a baseline for the measurements at higher refractive indices. This method was applied to the spectra present in figure 12 for nine different fluids with refractive indices between 1.333 and 1.490 ($n_D^{25ºC}$). The dark blue spectra spectra were obtained from the optical waveguide at a surface-to-core center distance of 2.5 μm, while the dark red spectra were obtained from the optical waveguide produced at a surface-to-core center distance of 19 μm. Each graph line in the transition in coloration from blue to red represents an increase in the waveguides depth of 0.5 µm. As can be seen, a loss peak is created by the excitation of a surface plasmon for every fluid tested. The wavelength at which the resonance condition occurs depends on the refractive index of the fluid, and the amplitude of the loss peak is not constant across the different optical waveguide depths and fluid refractive indices. It is visible that the peak amplitude is maximized for a given optical waveguide depth that changes depending on the refractive index of the fluid. From figure 12, it can be seen that this optimal waveguide depth increases with the increase in the fluid's refractive index. Basically, it has to do with the fact that when the resonant wavelength changes so does the mode confinement for each waveguide. For short wavelength resonances, the modes are better confined and therefore the waveguide has to be closer to the metallic film to compensate.

Therefore, the optimal waveguide depth at longer wavelengths is reached at depths greater than those at shorter wavelengths, with the performance of shallower waveguides still suffering from the loss in peak amplitude due to the absorption of the thin-films. Another aspect that can be visualized in this figure is the broadening of the peak as it red-shifts, hindering the determination of the resonance wavelength. Also, some issues are present in spectra of these devices, namely negative loss values and a peak/dip present at roughly 1150 nm in some of the spectra. Both issues are explained by slight variations in the positioning of the butt-coupling optical fibers, as they need to be manually aligned for every optical waveguide and the substrate removed and cleaned for every fluid. More specifically, the peak/dip present at 1150 nm arises from the subtraction of two spectra with slight differences in the region where the insertion losses undergoes a rapid variation (as is visible in Fig.11 at roughly the same wavelength).

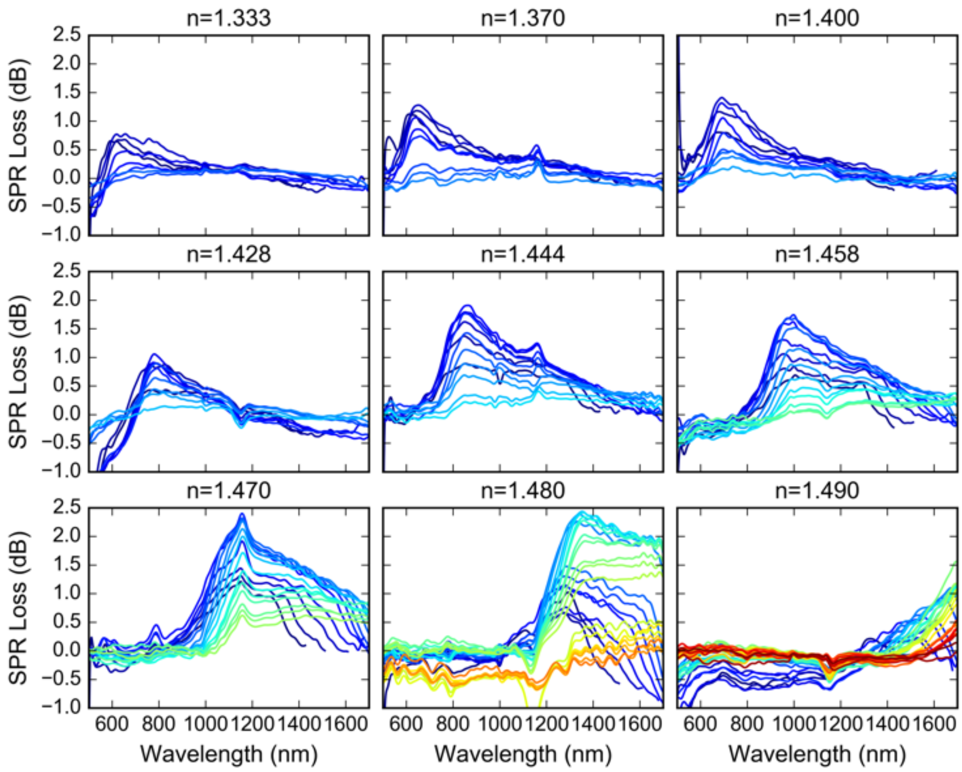

Fig. 12 - SPR induced loss spectra of the devices when exposed to fluids whose refractive index ranges between 1.333 and 1.490 ($n_D^{25ºC}$). The evolution from blue to red represents the transition from the shallowest optical waveguide to the deepest in steps of 0.5 µm.

In order to test the sensitivity of these devices to a change of the refractive index in the external fluid, one particular waveguide was selected for the remainder of this work. As it is impossible to choose one device that guarantees a maximum peak amplitude across the refractive index range of this study, the device chosen is a balance between the results found at both extremes of the refractive index range utilized. The device that better demonstrated this characteristic was the waveguide placed at a surface to core center distance of 4 µm. The loss peaks created by the excitation of a surface plasmon with the different fluids tested in this work are plotted in Fig. 13 (a). It should be noted that the loss spectra for a refractive index of 1.428 and 1.490 were manually adjusted in height in order for it to better represent the real result, i.e. the result that would be obtained in the absence of the coupling issues discussed before. In this figure, the red-shift of the loss peak is observable despite its increase in width interfering with the determination of the resonance wavelength. The resonance wavelength for each one of the fluids is plotted in Fig. 13 (b) as a function of their refractive index values (corrected for dispersion at the resonance wavelength). As can be seen, the resonance wavelength increases monotonically with the refractive index of the fluid in contact with the gold layer, following an exponential growth curve. The sensitivity of the device—obtained by the first derivative between two consecutive data points—is represented in the same figure, where it is seen to be negligible for refractive indices around that of water-based solutions, reaching values above 21000 nm/RIU for refractive indices closer to the refractive index of the glass substrate. Unfortunately, this inhibits the application of such devices in the determination of the concentration of a given analyte in water-based solutions. On the other hand, it opens a new window in refractive index sensing (between 1.44 and 1.50) beyond what is possible in conventional fused silica platforms. Due to the planar geometry of the device, this platform is especially suited for polymeric coatings whose refractive index falls in this window, as these coatings can then be used to sense a given parameter due to a variation in its own refractive index.

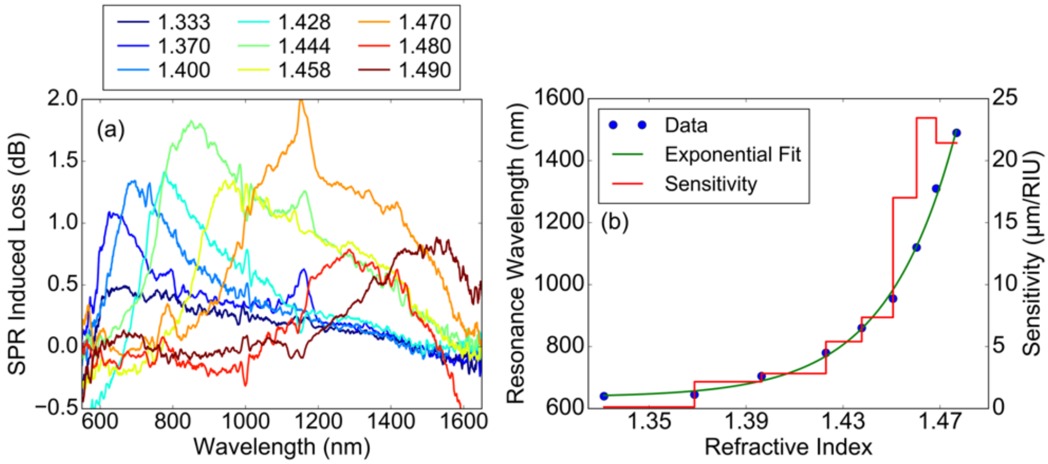

Fig. 13 - (a) SPR induced loss spectra obtained from an optical waveguide at a surface do core center distance of 4 µm for fluids whose refractive index ranges between 1.333 and 1.490 ($n_D^{25°C}$). (b) Resonance wavelength and sensitivity as a function of the fluid's refractive index.

5. CONCLUSIONS

The guiding properties of waveguides fabricated by femtosecond laser direct writing in fused silica and Eagle 2000 substrates were tested while varying processing parameters such as pulse energy, scan velocity, and annealing temperature (only for silica). In the case of fused silica waveguides, the insertion losses presented a mid-wavelength guiding band limited by increasingly higher losses at longer and shorter wavelengths. Coupling losses were found to control the long wavelength behaviour, and this type of losses increased whenever the pulse energy decreased, the scan velocity increased, or when the annealing temperature at which the waveguides were submitted was higher. The short wavelength behaviour was dominated by Rayleigh scattering that was seen to increase from ≈ 0.5 to 12.4 dB·cm^{-1}·µm^4 with scanning velocity, being attenuated with the application of thermal treatments and reaching a minimum of ≈ 0.08 dB·cm^{-1}·µm^4 when treated at 1000ºC. An almost wavelength independent baseline loss attributed to Mie scattering was observed, with values increasing from ≈ 0.2 to 0.65 dB/cm as pulse energy increased.

In the case of the alkaline earth boro-aluminosilicate glass (Eagle2000) waveguides, a similar guiding band limited by increasingly higher losses at longer and shorter wavelengths was visible. Coupling loss arising from the cut-off was found to control the long wavelength behavior, becoming negligible for pulse energies greater than 125 nJ. Added coupling loss due to modal mismatch was also present throughout the whole wavelength range. Regarding propagation loss, an almost wavelength independent baseline loss was also observed and attributed to Mie scattering. The former showed to be relatively independent of scan velocity, increasing from ≈ 0 to 0.3 dB/cm as pulse energy increased. Contrary to the case of fused silica, bulk absorption was also present, being responsible for the majority of the propagation loss at longer wavelengths. On the other end, loss at shorter wavelengths is mostly determined by Rayleigh scattering, which was found to decrease with increasing scan velocity from approximately 2 $dB\cdot cm^{-1}\cdot \mu m^4$ to a negligible value at this scale (<0.05 $dB\cdot cm^{-1}\cdot \mu m^4$). In sum, the fabrication of low-loss broadband optical waveguides was achieved in Eagle2000, with optimal results being obtained for very high scanning velocities (≈10 cm/s).

The excitation of surface plasmons was demonstrated in a gold thin-film deposited on top of optical waveguides fabricated at the surface of an Eagle2000 substrate. By testing different optical waveguide depths, it was possible to observe that the spectral characteristics of the device are highly dependent on the separation between the guided mode and the thin-film. It was also possible to conclude that the depth at which the optical waveguide is placed is critical to the performance of the device, as the loss peak created by the surface plasmon is not maximized at the same waveguide depth for different refractive indices. The sensitivity was seen to be negligible for fluids with refractive indices around that of water-based solutions, increasing dramatically for higher refractive indices and reaching values above 21000 nm/RIU for refractive indices close to the refractive index of the glass substrate.

REFERENCES

[1] K. M. Davis, K. Miura, N. Sugimoto, and K. Hirao, "Writing waveguides in glass with a femtosecond laser," *Opt. Lett.*, vol. 21, no. 21, pp. 1729-1731, Nov. 1996.

[2] S. M. Eaton, H. Zhang, and P. R. Herman, "Heat accumulation effects in femtosecond laser-written waveguides with variable repetition rate," *Opt. Express*, vol. 13, no. 12, pp. 4708-4716, Jun. 2005.

[3] H. Zhang, S. M. Eaton, and P. R. Herman, "Single-step writing of Bragg grating waveguides in fused silica with an externally modulated femtosecond fiber laser," *Opt. Lett.*, vol. 32, no. 17, pp. 2559-2561, Sep. 2007).

[4] S. M. Eaton, W. Chen, L. Zhang, H. Zhang, R. Iyer, J. S. Aitchison, and P. R. Herman, "Telecom-Band Directional Coupler Written With Femtosecond Fiber Laser," *IEEE Photon. Technol. Lett.*, vol. 18, no. 20, pp. 2174-2176, Oct. 2006

[5] V. A. Amorim, J. M. Maia, D. Alexandre, and P. V. S. Marques, "Optimization of Broadband Y-Junction Splitters in Fused Silica by Femtosecond Laser Writing,", *IEEE Photon. Technol. Lett.,* vol. 29, no. 7, pp. 619-622, Apr. 2017

[6] T. Calmano, J. Siebenmorgen, O. Hellmig, K. Petermann, and G. Huber, "Nd:YAG waveguide laser with 1.3 W output power, fabricated by direct femtosecond laser writing," *Appl. Phys. B*, vol. 100, no. 1, pp. 131-135, Jul. 2010.

[7] V. A. Amorim, J. M. Maia, D. Alexandre, and P. V. S. Marques, "Monolithic add-drop multiplexers in fused silica fabricated by femtosecond laser direct writing," *J. Light. Technol.,* vol. 35, no. 17, pp. 3615-3621, Sep. 2017.

[8] G. Douglass, F. Dreisow, S. Gross, and M. J. Withford, "Femtosecond laser written arrayed waveguide gratings with integrated photonic lanterns," *Opt. Express*, vol. 26, no. 2, pp. 1497-1505, Jan. 2018

[9] R. R. Thomson, H. T. Bookey, N. D. Psaila, A. Fender, S. Campbell, W. N. MacPherson, J. S. Barton, D. T. Reid, and A. K. Kar, "Ultrafast-laser inscription of a three dimensional fan-out device for multicore fiber coupling applications," *Opt. Express*, vol. 15, no. 18, pp. 11691-11697, Sep. 2007.

[10] J. M. Maia, V. A. Amorim, D. Alexandre, and P. V. S. Marques, "Real-time optical monitoring of etching reaction of microfluidic channel fabricated by femtosecond laser direct writing," *J. Light. Technol.,* vol. 35, no. 11, pp. 2291-2298, Jun. 2017

[11] A. Crespi, Y. Gu, B. Ngamsom, H. Hoekstra, C. Dongre, M. Pollnau, R. Ramponi, H. Vlekkert, P. Watts, G. Cerullo, and R. Osellame, "Three-dimensional Mach-Zehnder interferometer in a microfluidic chip for spatially-resolved label free detection," *Lab Chip*, vol. 10, no. 9, pp. 1167-1173, May 2010

[12] C. Caucheteur, T. Guo, and J. Albert, "Review of plasmonic fiber optic biochemical sensors: improving the limit of detection," *Anal. Bioanal. Chem.*, vol. 407, no. 14, pp. 3883-3897, May 2015

[13] M. Kim, D. J. Hwang, H. Jeon, K. Hiromatsu, and C. P. Grigoropoulos, "Single cell detection using a glass-based optofluidic device fabricated by femtosecond laser pulses," *Lab Chip*, vol. 9, no. 2, pp. 311-318, Jan. 2009

[14] R. R. Thomson, S. Campbell, I. J. Blewett, A. K. Kar, D. T. Reid, S. Shen, and A. Jha, "Active waveguide fabrication in erbium-doped oxyfluoride silicate glass using femtosecond pulses," *Appl. Phys. Lett.*, vol. 87, 121102, Sep. 2005

[15] L. Tong, R. R. Gattass, I. Maxwell, J. B. Ashcom, E. Mazur, “Optical loss measurements in femtosecond laser written waveguides in glass,” *Opt. Commun.*, vol. 259, pp. 626-630, Mar. 2006
[16] silica
[17] Eagle 2000
[18] P. G. Kazansky, W. Yang, E. Bricchi, J. Bovatsek, A. Arai, Y. Shimotsuma, K. Miura, and K. Hirao, “Quill writing with ultrashort light pulses in transparent materials” *Appl. Phys. Lett.*, vol. 90, no. 15, art. no. 151120, Apr. 2007
[19] J. W. Chan, T. Huser, S. Risbud, D. M. Krol, “Structural changes in fused silica after exposure to focused femtosecond laser pulses,” *Opt. Lett.*, vol. 26, no. 21, pp. 1726-1728, Nov. 2001.
[20] J. W. Chan, T. R. Huser, S. H. Risbud, D. M. Krol, “Modification of the fused silica glass network associated with waveguide fabrication using femtosecond laser pulses,” *Appl. Phys. A*, vol. 76, no. 3, pp. 367-372, Mar. 2003
[21] W. J. Reichman, D. M. Krol, L. Shah, F. Yoshino, A. Arai, S. M. Eaton, and P. R. Herman, “A spectroscopic comparison of femtosecond-laser-modified fused silica using kilohertz and megahertz laser systems,” *J. Appl. Phys.*, vol. 99, no. 12, 123112, Jul. 2006
[22] R D. J. Little, M. Ams, P. Dekker, G. D. Marshall, J. M. Dawes, and M. J. Withford, “Femtosecond laser modification of fused silica: the effect of writing polarization on Si-O ring structure,” *Opt. Express*, vol. 16, no. 24, pp. 20029-20037, Nov. 2008
[23] M. Sakakura, M. Terazima, Y. Shimotsuma, K. Miura, and K. Hirao, “Thermal and shock induced modification inside a sílica glass by focused femtosecond laser pulse,” *J. Appl. Phys.*, vol. 109, no. 2, 023503, Feb. 2011
[24] A. Champion and Y. Bellouard, “Direct volume variation measurements in fused silica specimens exposed to femtosecond laser,” *Opt. Mater. Express*, vol. 2, no. 6, pp. 789-798, May 2012
[25] J. J. Witcher, W. J. Reichman, L. B. Fletcher, N. W. Troy, and D. M. Krol, “Thermal annealing of femtosecond laser written structures in silica glass,” *Opt. Mater. Express*, vol. 3, no. 4, pp. 502-510, Mar. 2013
[26] L. Shah, A. Y. Arai, S. M. Eaton, and P. R. Herman, “Waveguide writing in fused silica with femtosecond fiber laser at 522 nm and 1 MHz repetition rate,” *Opt. Express*, vol. 13, no. 6, pp. 1999-2005, Apr. 2005
[27] S. M. Eaton, H. Zhang, M. L. Ng, J. Li, W. Chen, S. Ho, and P. R. Herman, “Transition from thermal diffusion to heat accumulation in high repetition rate femtosecond laser writing of buried optical waveguides,” *Opt. Express*, vol. 16, no. 13, pp. 9443-9458, Jun. 2008
[28] A. Arriola, S. Gross, N. Jovanovic, N. Charles, P. G. Tuthill, S. M. Olaizola, A. Fuerbach, and M. J. Withford, “Low bend loss waveguides enable compact, efficient 3D photonic chips,” *Opt. Express*, vol. 21, no. 3, pp. 2978-2986, Feb. 2013
[29] T. Meany, S. Gross, N. Jovanovic, A. Arriola, M. J. Steel, and M. J. Withford, “Towards low-loss lightwave circuits for non-classical optics at 800 nm and 1550 nm,” *Appl. Phys. A*, vol. 114, no. 1, pp. 113-118, Jan. 2014
[30] O. Humbach, H. Fabian, U. Grzesik, U. Haken, and W. Heitmann, “Analysis of OH absorption bands in synthetic silica,” *J. Non-Cryst. Solids*, vol. 203, pp. 19-26, Aug. 1996
[31] L. B. Glebov, and E. N. Boulos, “Absorption of iron and water in the Na_2O-CaO-MgO-SiO_2 glasses. II, Selection of intrinsic, ferric, and ferrous spectra in the visible and UV regions,” *J. Non-Cryst. Solids*, vol. 242, no. 1, pp. 49-62, Dec. 1998
[32] S. M. Eaton, W. Chen, H. Zhang, R. Iyer, J. Li, M. L. Ng, S. Ho, J. S. Aitchison, and P. R. Herman, “Spectral loss characterization of femtosecond written waveguides in glass with application to demultiplexing of 1300 and 1550 nm wavelengths,” *J. Light. Technol.*, vol. 27, no. 9, pp. 1079-1085, May 2009